

## Adsorption of an Azo Dye on Graphene Nanosheet: A Molecular Dynamics Simulation Study

S. Samiee<sup>a</sup>, F. Moosavi<sup>a</sup> and E.K. Goharshadi<sup>a,b,c,\*</sup>

<sup>a</sup>*Department of Chemistry, Faculty of Science, Ferdowsi University of Mashhad, Mashhad 9177948974, Iran*

<sup>b</sup>*Center of Nano Research, Ferdowsi University of Mashhad, Mashhad 9177948974, Iran*

<sup>c</sup>*Micro-Nano Technologies in Renewable Energies Center, Ferdowsi University of Mashhad, Mashhad 9177948974, Iran*

*(Received 6 March 2022, Accepted 14 May 2022)*

Molecular dynamics simulation was used to investigate the adsorption of a typical azo dye on a graphene nanosheet (GNS). The influence of temperature on the adsorption process was studied in the temperature range of 288.15 to 338.15 K. The structural, transport, and thermodynamic properties of dye and GNS were investigated during adsorption. The results showed that the potential of mean force becomes more negative by reaching dye molecule to GNS surface, which reflects the spontaneous adsorption of dye molecule on GNS. The structural studies showed that  $\pi$ - $\pi$  stacking between the benzene rings of dye and the GNS surface plays a key role for an efficient adsorption. The results showed that after adding GNS to the dye solution, the diffusion coefficient of dye decreased from  $2.718 \times 10^{-8} \text{ m}^2 \text{ s}^{-1}$  to  $1.755 \times 10^{-8} \text{ m}^2 \text{ s}^{-1}$  owing to adsorption. Both radial distribution function and density profile analysis showed that the interaction between water and dye weakens due to the presence of GNS. The isochoric heat capacity was calculated as  $24.85 \text{ J mol}^{-1} \text{ K}^{-1}$ . By increasing the temperature from 288.15 to 338.15 K, the adsorption energy decreased from  $-2.5070$  to  $-1.7302 \text{ kJ mol}^{-1}$ . The negative and low adsorption energies indicate that the dye was physically adsorbed on GNS.

**Keywords:** Graphene, Azo dye, Adsorption, Molecular dynamics simulation, Thermodynamic properties

### INTRODUCTION

Water pollution is a serious environmental concern. Industrial developments and population growth lead to release of the contaminants into the environment that increased the destructive and harmful effects of these pollutants [1]. Industrial effluents contain high concentration of chemicals such as hydrocarbon solvents, heavy metals, and dyes. Dyes are considered as one of the most important group of contaminants. Among various types of dyes, azo dyes threaten environment to a great extent due to their toxic nature, recalcitrant structures, and widespread usage in the textile industry. Therefore, the removal of azo dyes from effluents is an urgent need [2].

Up to now, several techniques such as oxidation,

ozonation, biological degradation, and adsorption have been used to remove dye molecules from colored effluents [3-9]. Among all available methods, adsorption is widely applied for water treatment because of its cost, flexibility, simplicity of design, and insensitivity to toxic pollutants [10]. Adsorption is a surface phenomenon where pollutants are adsorbed onto the surface of an adsorbent [11]. Several types of traditional adsorbents such as activated carbon, clay minerals, chelating agents, biosorbents, and chitosan/natural zeolites can remove dyes from aqueous solutions [12,13]. However, their low adsorption capacities and long adsorption equilibrium duration or period limit their applications [14]. To address these limitations, some nanomaterials (NMs) have been used as novel adsorbents [15]. NMs are superior adsorbents due to their small size, large surface area, and multiple

\*Corresponding author. E-mail: [gohari@um.ac.ir](mailto:gohari@um.ac.ir)

active sites [16]. Carbonaceous NMs as novel adsorbents have high adsorption capacity and selectivity for organic solutes in aqueous solutions [17-19]. Few examples of carbonaceous NMs are carbon nanotube, graphene, graphene oxide, graphene nanoribbons, and graphene quantum dots. Graphene is a perfect two-dimensional carbon sheet in which sp<sup>2</sup>-hybridized carbon atoms arranged in a hexagonal honeycomb lattice [16]. Among all outstanding properties of graphene, the large specific surface area (2630 m<sup>2</sup> g<sup>-1</sup>) and the flat structure make it an ideal adsorbent for removal of pollutants [17,20,21]. The out-of-plane  $\pi$  bonds in graphene can form  $\pi$ - $\pi$  stacking interactions with delocalized network of electrons in aromatic compounds [22,23].

Liu *et al.* [24] investigated the adsorption of methylene blue (MB) as a cationic dye from water by graphene oxide (GO) using molecular dynamics (MD) simulation. Their study revealed that MB cations quickly aggregate around the GO in water.

Hezarkhani and Ghadari [25] explored the binding properties of azo dyes to a nitrogen doped GO using computational modelling. MD simulation studies showed that the binding of azo dyes to the surface of the nitrogen-doped GO is mainly performed by van der Waals interactions.

Yadav *et al.* [26] studied the simultaneous adsorption of MB and arsenic (III) on graphene, boron nitride, and boron carbon nitride nanosheets using MD simulation. They found graphene among NMs is superior for simultaneous adsorption of MB and arsenic (III).

The main goal of the present study is to investigate the adsorption of an azo dye on graphene nanosheet (GNS) via MD simulation at different temperatures. A pristine GNS was considered as an adsorbent. For the first time, the current research reports the structural, thermodynamic, and transport properties of GNS and azo dye aqueous solution during adsorption by conducting a series of MD simulations.

## METHODOLOGY AND SIMULATION DETAILS

MD simulations were performed by DL\_POLY 2.17

**Table 1.** The LJ Parameters for Similar Atoms

Atom	$\sigma$ (Å)	$\epsilon$ (kJ mol <sup>-1</sup> )
N	3.26	0.324
C	3.40	0.233
S	3.59	1.439
O	3.03	0.400
Na	2.80	2.092
H	2.85	0.064

simulation package [27]. The carbon atoms in rigid graphene sheet were modelled as uncharged Lennard-Jones (LJ) spheres with  $\sigma_{cc} = 3.40$  Å and  $\epsilon_{cc} = 0.233$  kJ mol<sup>-1</sup> [28]. Azo dye molecule was described by the explicit atomistic model in DREIDING force field. Ewald summation was applied to compute the long-range electrostatic interactions whereas van der Waals (vdW) interactions were treated with LJ potential. The LJ parameters for the similar atoms are reported in Table 1. The water-graphene, water-dye, and dye-graphene interaction parameters are  $\sigma_{ij}$  and  $\epsilon_{ij}$  derived from the Lorentz-Berthelot combining rules [29]:

$$\sigma_{ij} = (\sigma_{ii} + \sigma_{jj})/2 \quad (1)$$

$$\epsilon_{ij} = (\epsilon_{ii}\epsilon_{jj})^{1/2} \quad (2)$$

In above formulations, the subscripts of ii and jj belong to the pure compounds. The GNS in this work consists of 1680 carbon atoms symbolized by C\_2 hereafter. Dye solution was prepared by adding one dye molecule into 1339 water molecules to construct a dilute solution with  $x_{\text{dye}} = 7.46 \times 10^{-4}$ . Figures 1a and 1b show the structures of GNS and dye molecule, respectively. Density functional theory (DFT) was used to obtain the optimized structure and atomic charges of dye molecule. These computations were done at the B3LYP/6-31+G\* level of theory using Gaussian 03 package [30]. Table S1 gives the equilibrium bond lengths, equilibrium angles, and natural bond orbital atomic charges of dye molecule. The frequency calculation was conducted to ensure that the dye is in its local minimum. It is worth to mention that GNS in Fig. 1a is large enough to provide an appropriate surface for adsorption of a big molecule like an

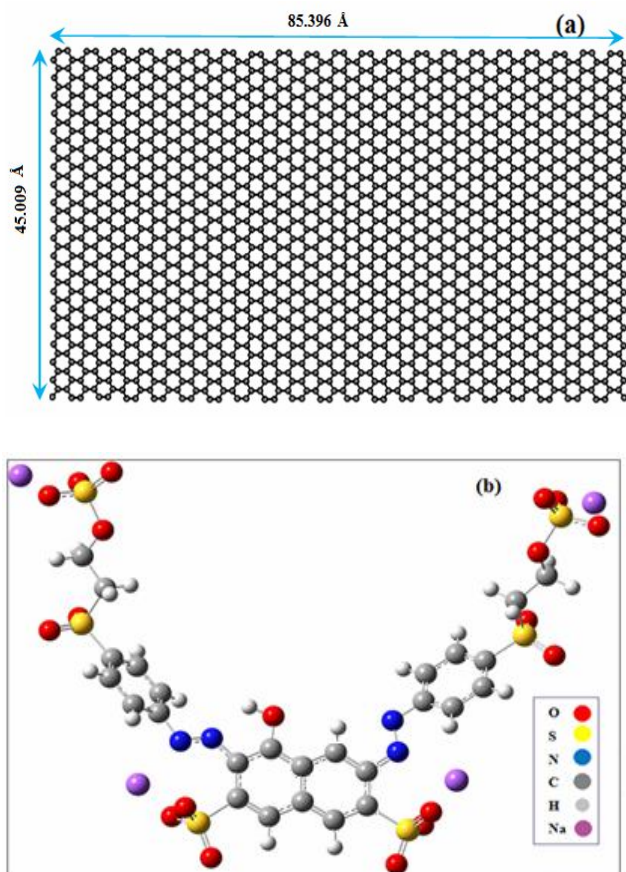


**Fig. 1.** The structure of (a) GNS and (b) azo dye.

azo dye. For the case of water, simple point charge (SPC) potential was applied with atomic charges computed at B3LYP/6-31+G\* level of theory. Table S2 reports atomic charges computed for the water molecule.

Simulations were carried out in  $NVT$  ensemble. The equations of motion were integrated with a time step of 0.1 fs using Leapfrog Verlet integration algorithm [31]. The velocity-rescaled Berendsen thermostat with a relaxation time of 1 ps was implemented to maintain the system at a constant temperature. Periodic boundary conditions were used in all three directions. The dimensions of the simulation box were  $90.639 \times 90.693 \times 90.693 \text{ \AA}^3$ . The cut off distance for non-bonded interactions was considered 15 Å. All calculations were performed after the system reached to equilibrium, *i.e.*, the system achieved constant energy and temperature. After the equilibrium, the

Berendsen thermostat was turned off. Three separate sets of simulation for GNS, dye solution, and mixed system (dye solution + GNS) were carried out. These simulations were the same in all details except the number of steps. The simulation temperature was varied from 288.15 to 338.15 K.

## RESULTS AND DISCUSSION

Adsorption of dye molecule on GNS surface was investigated by performing three different simulations for the GNS, the dye solution (1 dye molecule + 1339 water molecules,  $x_{\text{dye}} = 7.46 \times 10^{-4}$ ), and the mixed system (the dye solution with  $x_{\text{dye}} = 7.46 \times 10^{-4}$  + GNS), respectively. In the following sections, the structural, thermodynamic, and transport properties of the dye molecule before and after adsorption on the GNS surface were studied.

### Structural Properties

The radial distribution function (RDF) acts as a link for connecting macroscopic thermodynamic properties to interparticle interactions of a substance [32]. Figure 2 shows the radial distribution function (RDF) for the GNS atoms. The appearance of the sharp peaks is consistent with the long-range order of solid systems. The RDF is zero for short distances (less than 1.245 Å) due to strong repulsive forces.

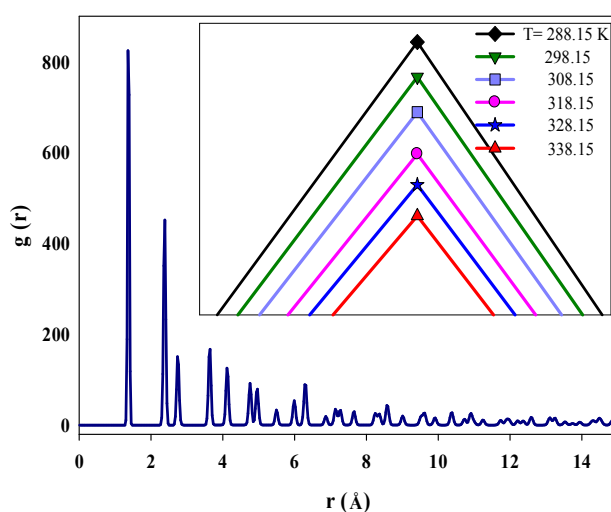


**Fig. 2.** The RDF of GNS (inset: the effect of temperature on the first RDF peak).

The inset in Fig. 2 shows the effect of temperature on the first RDF peak of the GNS. As temperature increased, the intensity of peaks decreased due to an increase in thermal motions and a decrease in pair correlations. However, the position of the RDF peaks did not change.

In order to further understand the interaction between the dye atoms and solvent, the RDFs of water molecules around dye atoms were investigated. The label of dye atoms is shown in Table 2. Figure 3 shows the RDFs of different atoms of dye (C\_3, C\_R, N\_R, O\_2, O\_3, and S\_3) with respect to hydrogen of water molecules. The appearance of a few damped oscillating peaks in Fig. 3 is a characteristic feature of liquids and confirms the existence of short-range interactions. The overall RDF distributions for C\_3 and S\_3 in dye molecule were relatively flat corresponding to weak solvation interactions. On the other hand, there were significant solvation peaks for N\_R, O\_2, O\_3, and C\_R atoms at 2.70, 2.73, 2.65, and 3.92 Å, respectively; this is due to their ability to form the strong interactions with hydrogen atoms of water molecules.

The adsorption of dye on GNS can be monitored by studying the correlations between different atoms of dye and graphene surface. All possible correlations between dye atoms (O\_2, O\_3, S\_3, N\_R, C\_R, and C\_3) and GNS surface were considered. Figure 4 shows that all atoms of dye have effective interactions with the GNS in the distance range between 4.0 to 5.1 Å. Among different atoms of dye, C\_R, C\_3, O\_2, and S\_3 atoms were relatively close to the GNS surface. The close distance between C\_R and GNS may be related to the formation of  $\pi$ - $\pi$  interactions with GNS. When the spacing between the two neighbouring molecules is approximately less than 4.5 Å (the characteristic length for the  $\pi$ - $\pi$  stacking distance), it is expected that the interaction occurs due to this special type of interaction. Since the GNS surface in this work has no charge, the only driving force for adsorption of dye on GNS was  $\pi$ - $\pi$  stacking interactions. Therefore, during the simulation time, dye molecule twisted and folded to reach or attain the proper orientation for the  $\pi$ - $\pi$  interactions. As a result of twisting, O\_2 and S\_3 atoms of dye, which were connected to the benzene rings, also became closer to the GNS surface.

**Table 2.** The Labels of Dye Atoms

Label	Description
N_R	Nitrogen atoms bonded to ring
N_3	Nitrogen atoms with $sp^3$ hybridization
C_3	Carbon atoms with $sp^3$ hybridization
C_R	Carbon atoms bonded to ring
O_2	Oxygen atoms with $sp^2$ hybridization
O_3	Oxygen atoms with $sp^3$ hybridization
S_3	Sulfur atoms with $sp^3$ hybridization
Na	Sodium atoms

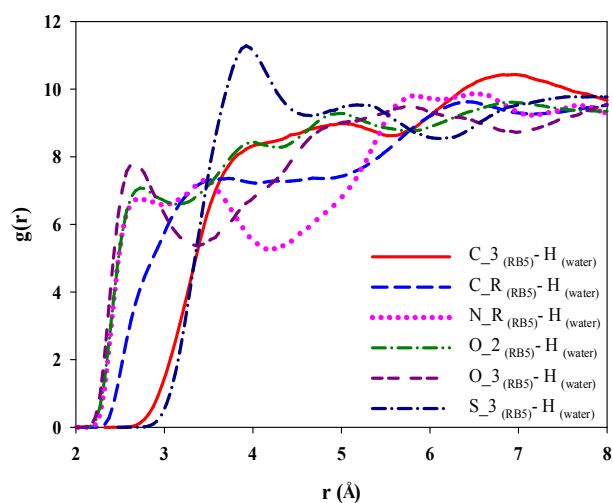


**Fig. 3.** The correlation between different dye atoms and hydrogen of water molecules.

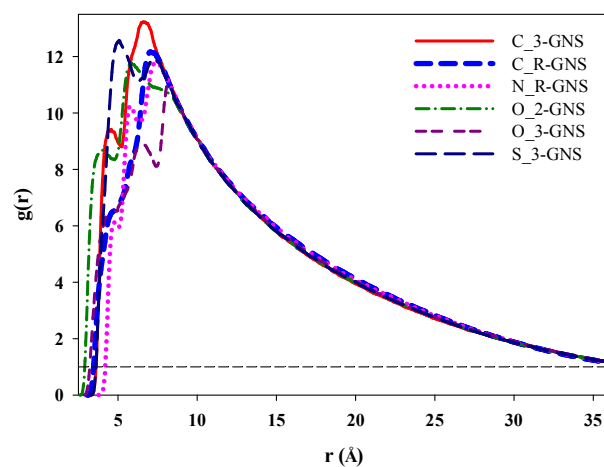


**Fig. 4.** The RDF of different dye atoms and GNS.

From the RDFs, we obtained potential of mean force (PMF),  $W(r)$  between the dye atoms and the GNS surface.  $W(r)$  is defined as [33]:

$$W(r) = -kT \ln g(r) \quad (3)$$

The PMF plot is shown in Fig. 5. When the RDF is larger than unity, the corresponding effective pair potential is negative (attractive). The  $W(r)$  is positive (repulsive) when the RDF is less than unity. Using the PMF curves, we can evaluate the free energy of atoms during the adsorption process. From Fig. 5, the free energy of all dye atoms decreased by the movement of the dye molecule from aqueous solution to the graphene surface. When dye atoms reached to the graphene surface, the amount of  $W(r)$  became more negative. It confirms the spontaneous adsorption of dye on GNS. This behavior again reflects that the  $\pi$ - $\pi$  stacking interaction between dye molecule and graphene is the driving force for the adsorption.

The pair correlation function between the oxygen atoms of dye (O\_2) and the hydrogen atoms of water (HW) at 298.15 K is shown in Fig. 6. The area below the curves is a measure of the total interactions. Before adding GNS, the water molecules were near the O\_2 atoms of dye due to the strong hydrogen bonds (HB). After adding graphene, O\_2 atoms were hindered from one side due to the adsorption on GNS, and the number of HB interactions significantly reduced. Therefore, lower RDF plot of mixed system can be related to the adsorption of dye on the GNS, which weakens the HB interactions between water and dye.

Investigation of changes in atomic density during the simulation is useful to elucidate the preferred orientation of the dye molecule toward the GNS. Figures 7a and 7b show the atomic densities in Z-direction of the simulation box before and after adding GNS to the dye solution at 298.15 K, respectively. Before adding GNS, there was no distinct boundary between curves and there were random distributions. In Z-density profile, outer lines may be attributed to atoms orientated toward solid surface while other atoms orientated toward solution [34]. After adding the GNS, the density of aromatic part of the dye (C\_R) and the oxygen of carbonyl group (O\_2) were obviously separated from others and located in the external lines of diagram. Formation of  $\pi$ - $\pi$  interactions is favourable due to

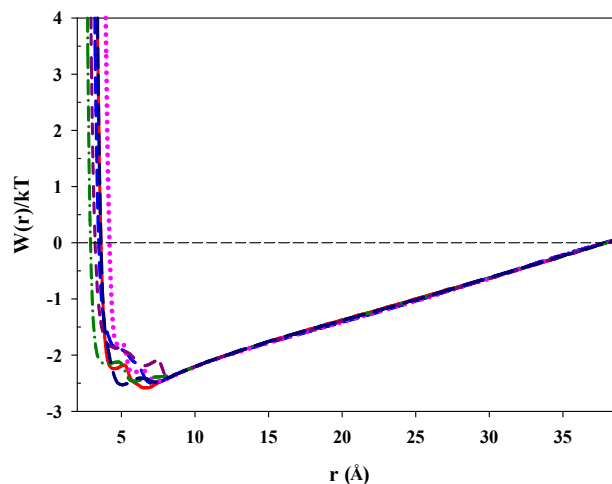


**Fig. 5.** The PMF curves for different atoms of dye during the adsorption of dye molecule on GNS surface. The symbols are the same as Fig. 4.

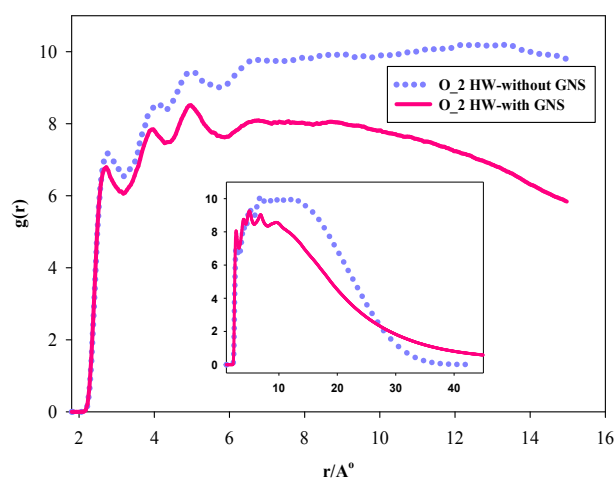


**Fig. 6.** The RDF plot of O\_2 and HW correlation in the absence and presence of GNS (inset: the same plot for cut off distance of 45 Å).

the presence of delocalized  $\pi$ -electrons of GNS. Therefore, the dye molecule was folded in such a way to orient C\_R atoms in the closest distance with respect to the surface. This facilitates the formation of  $\pi$ - $\pi$  stacking interactions between the benzene rings of the dye and the GNS. As a result of this folding, O\_2 atoms are also located in a closer distance to the graphene surface. Peaks of other dye atoms

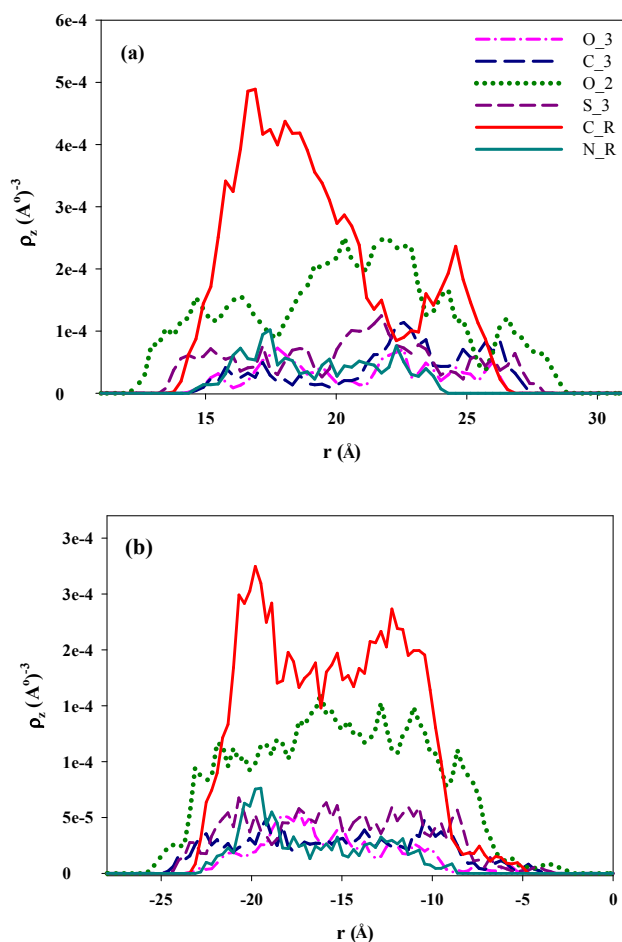


**Fig. 7.** The Z-density of different atoms of dye (a) before and (b) after adding GNS. The symbols in (a) and (b) are the same

(except O\_2 and C\_R) were inside the Z-density plot, showing that these atoms were oriented towards the solution rather than toward the GNS surface.

The snapshots at different time intervals of simulation are illustrated in Fig. 8. The initial structure of the dye molecule on the GNS surface is shown in Fig. 8a. At initial step, dye molecule was completely intact. After passing 120 ps from simulation, dye molecule came closer to the graphene surface and began twisting to achieve the optimum structure (Fig. 8b). When the simulation time approached to 1.8 ns, dye molecule attained to an optimum structure in which the benzene rings oriented and twisted to

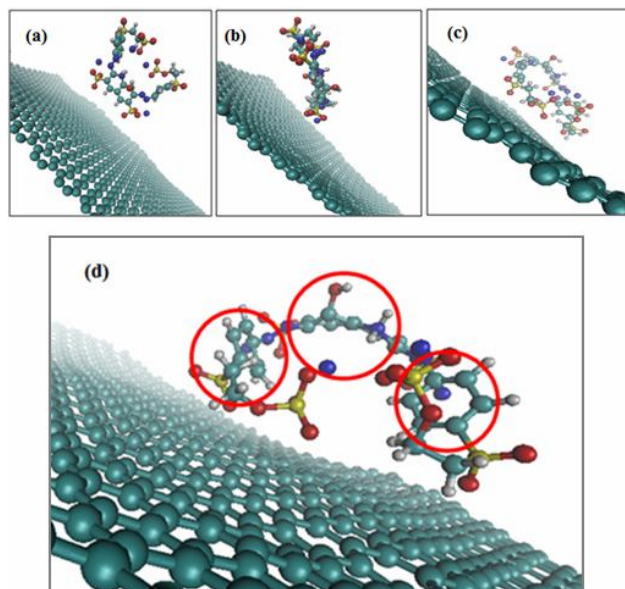


**Fig. 8.** Snapshots of dye direction to GNS surface at (a)  $t = 0$  ps, (b)  $t = 120$  ps, (c)  $t = 1.8$  ns, and (d) formation of  $\pi$ - $\pi$  stacking interactions between benzene rings of dye molecule and GNS surface at 298.15 K.

construct  $\pi$ - $\pi$  stacking with the graphene surface. As shown in Fig. 8c, during the adsorption of dye on the GNS, the structure of dye did not change. Also, Fig. 8c shows GNS was not degraded during the simulation. For simplicity, water molecules are not shown in this figure.

### Transport Properties

The mean square displacement (MSD) is used to calculate transport properties of a system. MSD can be related to diffusion coefficient,  $D$ , by the Einstein relation [35]:

$$MSD = \left\langle \left| \vec{r}(t) - \vec{r}(0) \right|^2 \right\rangle \quad (4)$$

$$D = \lim_{t \rightarrow \infty} \frac{\left\langle \left| \vec{r}(t) - \vec{r}(0) \right|^2 \right\rangle}{6t} \quad (5)$$

In this formulation, the  $r(0)$  and  $r(t)$  represent the position vector of the central mass of a molecule at initial time and at time  $t$ , respectively.

In a solid system, atoms are approximately fixed at their positions. Hence, MSD cannot be applied for a solid system like GNS. Temperature dependence of MSD for the mixed system was studied at different temperatures from 288.15 to 338.15 K (Fig. 9). The results show that by increasing the temperature, the slope of the MSD increases. The diffusion coefficients of the mixed system obtained from the MSD plots and the correlation factors ( $R^2$ ) are listed in Table 3. As shown in this table, by increasing the temperature, the diffusion coefficient increased due to the increased random motions.

The correlation between the diffusion coefficient and temperature is given by the following equation:

$$\ln D = \ln D_o - \frac{E_{diff}}{RT} \quad (4)$$

Here,  $D_o$  is diffusion coefficient at very high temperature,  $R$  is the gas constant, and  $T$  is absolute temperature.  $E_{diff}$  is the activation energy of migration. The calculated  $E_{diff}$  and  $D_o$  were 19.927 kJ mol<sup>-1</sup> and  $5.159 \times 10^{-5}$  m<sup>2</sup> s<sup>-1</sup>, respectively (using Fig. 10).

Figure 11 demonstrates that there is a significant difference between the MSD of dye before and after adsorption. Before adding graphene, the dye molecule could freely diffuse among the water molecules of the system. Adsorption of dye molecule on the graphene surface slowed down the motions of the dye molecule, which in turn decreased the diffusion coefficient and MSD. The diffusion coefficient of dye decreased from  $2.718 \times 10^{-8}$  m<sup>2</sup> s<sup>-1</sup> to  $1.755 \times 10^{-8}$  m<sup>2</sup> s<sup>-1</sup> after adding graphene at 298.15 K. This reduction is a good evidence for adsorption of dye on graphene surface.

### Thermodynamic Properties

By applying simulations based on  $NVT$  ensemble, the isochoric heat capacity,  $C_v$ , can be calculated. The isochoric heat capacity is expressed as:

$$C_v = \left( \frac{\partial E}{\partial T} \right)_v \quad (5)$$

Here,  $E$  is the total energy. The value of  $C_v$  was from the slope of graph  $E$  versus  $T$  (Fig. S1). The calculated  $C_v$  was 24.85 J mol<sup>-1</sup> K<sup>-1</sup>, which is in a good agreement with the literature value (24.98 J mol<sup>-1</sup> K<sup>-1</sup>) [36,37].

**Table 3.** The Diffusion Coefficients of Mixed System at Different Temperatures

T (K)	$D \times 10^{-8}$ (m <sup>2</sup> s <sup>-1</sup> )	$R^2$
288.15	1.9654	0.9979
298.15	1.7549	0.9998
308.15	2.0309	0.9998
318.15	2.7536	0.9999
328.15	3.3668	1.0000

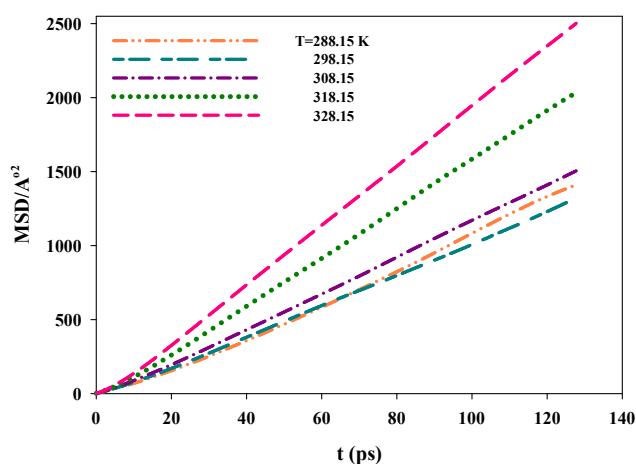


**Fig. 9.** The MSD of mixed system at different temperatures.

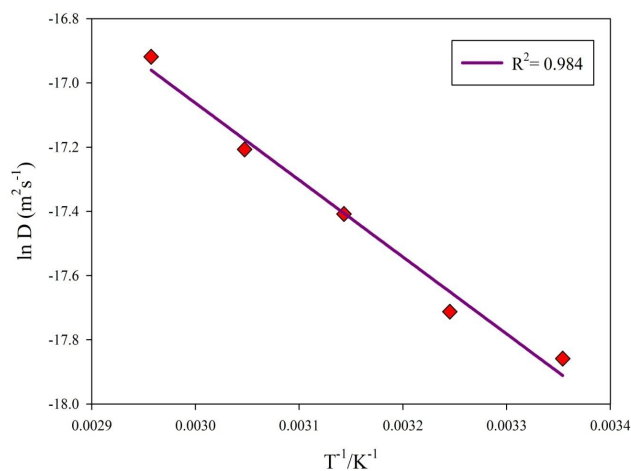


**Fig. 10.** The correlation between diffusion coefficient and temperature.

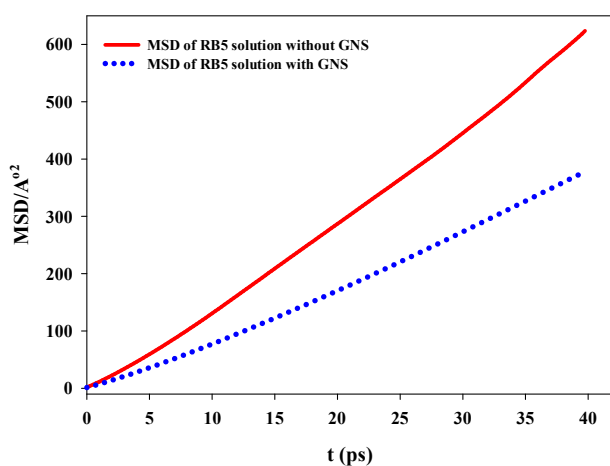


**Fig. 11.** The MSD of dye solution before and after adding GNS at 298.15 K

The values of  $C_v$  for the dye and the mixed solutions are shown in Table 4. According to this table, the order of isochoric heat capacity for different systems is as follows: dye solution > mixed system > GNS. The maximum  $C_v$  was obtained for the dye solution; this is due to the presence of strong electrostatic and HB interactions between water and dye. In the mixed system, electrostatic interactions decreased compared to the dye solution because of the presence of GNS; the surface prevents the formation of strong HB between water and dye. On the other hand,  $\pi$ - $\pi$  interactions compensated the decrease in electrostatic interactions to some extent. Therefore, the  $C_v$  of the mixed system was intermediate between dye solution and GNS pure systems and its value was closer to the dye solution than to the GNS. In the GNS system, there was neither electrostatic nor  $\pi$ - $\pi$  interactions and hence, the minimum value of  $C_v$  was obtained for this system.

Adsorption energy,  $E_{ads}$ , can be calculated using the following equation:

$$E_{ads} = E_{GNS+dye} - E_{GNS} - E_{dye} \quad (6)$$

Here,  $E_{GNS+dye}$ ,  $E_{GNS}$ , and  $E_{dye}$  are the total energy of the mixed system, total energy of the GNS, and total energy of the dye solution, respectively. The values of  $E_{ads}$  at different temperatures are shown in Table 5. The negative values of

**Table 4.** Isochoric Heat Capacity of GNS, Dye Solution, and Mixed System at the Temperature Range of 288.15 to 338.15 K

Sample	$C_v$ ( $J mol^{-1} K^{-1}$ )	$R^2$
GNS	24.85	1.000
Dye	37.28	0.999
Mixed system	35.89	0.999

**Table 5.** Adsorption Energies of Dye Molecule on GNS at Different Temperatures

T (K)	$E_{ads}$ ( $kJ mol^{-1}$ )
288.15	-2.5070
298.15	-2.4318
308.15	-2.3826
318.15	-2.1876
328.15	-2.1577
338.15	-1.7302

$E_{ads}$  indicated that adsorption of dye molecule on the surface is thermodynamically favorable. The small value of the adsorption energy indicated the physisorption of dye molecule on the GNS. Dye molecule was adsorbed on GNS via weak van der Waals and  $\pi$ - $\pi$  stacking interactions. The adsorption was more favorable at lower temperatures. By increasing temperature, random motions increased and adsorption of dye molecule on GNS surface weakened.

## CONCLUSIONS

MD simulation was performed to investigate the adsorption of an azo dye on GNS. Separate sets of MD simulations were performed on GNS, dye solution, and the mixed system. The MD simulations were performed in the temperature range of 288.15 to 338.15 K. The structural, transport, and thermodynamic properties of adsorption were obtained. The main conclusions are summarized as follows:

1. The results confirmed the adsorption of dye on the GNS. The diffusion coefficient of the mixed system ( $1.755 \times 10^{-8} \text{ m}^2 \text{ s}^{-1}$ ) is less than that of dye solution ( $2.718 \times 10^{-8} \text{ m}^2 \text{ s}^{-1}$ ) at 298.15 K due to the effective interactions between GNS and the dye molecule.
2. The free energy of atoms was evaluated during the adsorption process using the PMF curves. The results showed that the free energy of all dye atoms decreases by transferring dye molecule from the aqueous solution to the graphene surface. When dye atoms are close to the graphene surface, the  $W(r)$  is more negative. This confirm that the adsorption of dye on the GNS is spontaneous.
3. Dye is adsorbed physically on the GNS since the values of adsorption energy are low and negative.
4. The Z-density profiles were used to study the orientation in interfacial region and confirmed that dye atoms are re-oriented from rings (C\_R) and O\_2 atoms toward the graphene surface to form a  $\pi$ - $\pi$  stacking.

## ACKNOWLEDGMENTS

The authors appreciate Ferdowsi University of Mashhad for financial supporting of this project (3/23032).

## REFERENCES

- [1] Mahvelati-Shamsabadi, T.; Goharshadi, E. K.; Shafae, M.; Niazi, Z., ZnS@reduced graphene oxide nanocomposite as an effective sunlight driven photocatalyst for degradation of reactive black 5: A mechanistic approach. *Sep. Purif. Technol.* **2018**, *202*, 326-334. <https://doi.org/10.1016/j.seppur.2018.04.001>.
- [2] Asadi, F.; Goharshadi, E. K.; Sadeghinia, M., Highly efficient solar-catalytic degradation of reactive black 5 dye using mesoporous plasmonic Ag/G-C<sub>3</sub>N<sub>4</sub> nanocomposites. *Chem. Select* **2020**, *5*, 2735-2745. <https://doi.org/10.1002/slct.201904730>.
- [3] Goharshadi, E. K.; Hadadian, M.; Mahdi, M.; Azizi-Toupanloo, H., Photocatalytic degradation of reactive black 5 azo dye by zinc sulfide quantum dots prepared by a sonochemical method. *Mater. Sci. Semicond. Process.* **2013**, *16*. <https://doi.org/10.1016/j.mssp.2013.03.005>.
- [4] Ahmad, A.; Mohd-Setapar, S. H.; Chuong, C. S.; Khatoon, A.; Wani, W. A.; Kumar, R.; Rafatullah, M., Recent advances in new generation dye removal technologies: Novel search for approaches to reprocess wastewater. *RSC Adv.* **2015**, *5*, 30801-30818. DOI: <https://doi.org/10.1039/C4RA16959J>.
- [5] Katheresan, V.; Kandedo, J.; Lau, S. Y., Efficiency of various recent wastewater dye removal methods: A Review. *J. Environ. Chem. Eng.* **2018**, *6*, 4676-4697. <https://doi.org/10.1016/j.jece.2018.06.060>.
- [6] Pavithra, K. G.; Jaikumar, V., Removal of colorants from wastewater: A review on sources and treatment strategies. *J. Ind. Eng. Chem.* **2019**, *75*, 1-19. <https://doi.org/10.1016/j.jiec.2019.02.011>.
- [7] Selvaraj, V.; Karthika, T. S.; Mansiya, C.; Alagar, M., An over review on recently developed techniques, an over review on recently developed techniques, mechanisms and intermediate involved in the advanced azo dye degradation for industrial applications. *J. Mol. Struct.* **2021**, *1224*, 129195. <https://doi.org/10.1016/j.molstruc.2020.129195>.
- [8] Dutta, S.; Bhattacharjee, J., A Comparative Study between Physicochemical and Biological Methods for Effective Removal of Textile Dye from Wastewater. In *Development in Wastewater Treatment Research and Processes*; Elsevier, **2022**; pp. 1-21. <https://doi.org/10.1016/B978-0-323-85657-7.00003-1>.
- [9] Al-Gheethi, A. A.; Azhar, Q. M.; Kumar, P. S.; Yusuf, A. A.; Al-Buriah, A. K.; Mohamed, R. M. S. R.; Al-Shaibani, M. M., Sustainable approaches for removing rhodamine B dye using agricultural waste adsorbents: A Review. *Chemosphere* **2022**, *287*, 132080. <https://doi.org/10.1016/j.chemosphere.2021.132080>.
- [10] Yagub, M. T.; Sen, T. K.; Afroze, S.; Ang, H. M., Dye and its removal from aqueous solution by sorption: A Review. *Adv. Colloid Interface Sci.* **2014**, *209*, 172-184. <https://doi.org/10.1016/j.cis.2014.04.002>.
- [11] Rathi, B. S.; Kumar, P. S., Application of sorption process for effective removal of emerging contaminants from water and wastewater. *Environ. Pollut.* **2021**, *280*, 116995. <https://doi.org/10.1016/j.envpol.2021.116995>.

- [12] Wang, J.; Chen, C., Chitosan-based biosorbents: modification and application for biosorption of heavy metals and radionuclides. *Bioresour. Technol.* **2014**, *160*, 129-141. <https://doi.org/10.1016/j.biortech.2013.12.110>.
- [13] Han, H.; Rafiq, M. K.; Zhou, T.; Xu, R.; Mašek, O.; Li, X., A critical review of clay-based composites with enhanced sorption performance for metal and organic pollutants. *J. Hazard. Mater.* **2019**, *369*, 780-796. <https://doi.org/10.1016/j.jhazmat.2019.02.003>.
- [14] Goharshadi, E. K.; Moghaddam, M. B., Adsorption of hexavalent chromium ions from aqueous solution by graphene nanosheets: Kinetic and thermodynamic studies. *Int. J. Environ. Sci. Technol.* **2015**, *12*, <https://doi.org/10.1007/s13762-014-0748-z>. 10.1007/s13762-014-0748-z.
- [15] Lashen, Z. M.; Shams, M. S.; El-Sheshtawy, H. S.; Slaný, M.; Antoniadis, V.; Yang, X.; Sharma, G.; Rinklebe, J.; Shaheen, S. M.; Elmahdy, S. M., Remediation of Cd and Cu contaminated water and soil using novel nanomaterials derived from sugar beet processing-and clay brick factory-solid wastes. *J. Hazard. Mater.* **2022**, 128205. <https://doi.org/10.1016/j.jhazmat.2021.128205>.
- [16] Cai, Z.; Sun, Y.; Liu, W.; Pan, F.; Sun, P.; Fu, J., An overview of nanomaterials applied for removing dyes from wastewater. *Environ. Sci. Pollut. Res.* **2017**, *24*, 15882-15904. 10.1007/s11356-017-9003-8.
- [17] Samiee, S.; Goharshadi, E. K., Graphene nanosheets as efficient adsorbent for an azo dye removal: Kinetic and thermodynamic studies. *J. Nanoparticle Res.* **2014**, *16*, 2542. <https://doi.org/10.1007/s11051-014-2542-8>.
- [18] Rout, D. R.; Jena, H. M., Removal of phenol from aqueous solution using reduced graphene oxide as adsorbent: Isotherm, kinetic, and thermodynamic studies. *Environ. Sci. Pollut. Res.* **2022**, 1-15. <https://doi.org/10.1007/s11356-021-17944-y>.
- [19] Khoshnam, F.; Zargar, B.; Moghadam, M. R., Adsorption and removal of ametryn using graphene oxide nano-sheets from farm waste water and optimization using response surface methodology. *J. Iran. Chem. Soc.* **2019**, *16*, 1383-1390. <https://doi.org/10.1007/s13738-019-01621-6>.
- [20] Yu, J. -G.; Yu, L. -Y.; Yang, H.; Liu, Q.; Chen, X. -H.; Jiang, X. -Y.; Chen, X. -Q.; Jiao, F. -P., Graphene nanosheets as novel adsorbents in adsorption preconcentration and removal of gases, organic compounds and metal ions. *Sci. Total Environ.* **2015**, *502*, 70-79. <https://doi.org/10.1016/j.scitotenv.2014.08.077>.
- [21] Hadadian, M.; Goharshadi, E. K.; Fard, M. M.; Ahmadzadeh, H., Synergistic effect of graphene nanosheets and zinc oxide nanoparticles for effective adsorption of Ni(II) ions from aqueous solutions, *Appl. Phys. A Mater. Sci. Process.* **2018**, *124*, 239. <https://doi.org/10.1007/s00339-018-1664-8>.
- [22] Yang, Y.; Han, C.; Jiang, B.; Iocozzia, J.; He, C.; Shi, D.; Jiang, T.; Lin, Z., Graphene-based materials with tailored nanostructures for energy conversion and storage. *Mater. Sci. Eng. R Reports* **2016**, *102*, 1-72. <https://doi.org/10.1016/j.mser.2015.12.003>.
- [23] Kolev, S. K.; Aleksandrov, H. A.; Atanasov, V. A.; Popov, V. N.; Milenov, T. I., Interaction of graphene with out-of-plane aromatic hydrocarbons. *J. Phys. Chem. C* **2019**, *123*, 21448-21456. <https://doi.org/10.1021/acs.jpcc.9b03550>.
- [24] Liu, J.; Li, P.; Xiao, H.; Zhang, Y.; Shi, X.; Lü, X.; Chen, X., Understanding flocculation mechanism of graphene oxide for organic dyes from water: Experimental and molecular dynamics simulation, *AIP Adv.* **2015**, *5*, 117151. <https://doi.org/10.1063/1.4936846>.
- [25] Hezarkhani, M.; Ghadari, R., Exploration of the binding properties of the azo dye pollutants with nitrogen-doped graphene oxide by computational modeling for wastewater treatment improvement, *Chem. Select* **2019**, *4*, 5968-5978.
- [26] Yadav, A.; Dindorkar, S. S.; Ramiseti, S. B.; Sinha, N., Simultaneous adsorption of methylene blue and arsenic on graphene, boron nitride and boron carbon nitride nanosheets: Insights from molecular simulations, *J. Water Process Eng.* **2022**, *46*, 102653. <https://doi.org/https://doi.org/10.1016/j.jwpe.2022.102653>.
- [27] Smith, W.; Todorov, I. T.; Leslie, M., The DL\_POLY molecular dynamics package. *Zeitschrift Für Krist. Mater.* **2005**, *220*, 563-566.

- <https://doi.org/10.1524/zkri.220.5.563.65076>.
- [28] Cheng, A.; Steele, W. A., Computer simulation of ammonia on graphite. I. Low temperature structure of monolayer and bilayer films. *J. Chem. Phys.* **1990**, *92*, 3858-3866. <https://doi.org/10.1063/1.458562>.
- [29] Mahdizadeh, S. J.; Goharshadi, E. K., Hydrogen storage on silicon, carbon, and silicon carbide nanotubes: A combined quantum mechanics and grand canonical monte carlo simulation study, *Int. J. Hydrogen Energy* **2014**, *39*, 1719-1731. <https://doi.org/10.1016/j.ijhydene.2013.11.037>.
- [30] Frisch, M. J.; Trucks, G. W.; Schlegel, H. B.; Scuseria, G. E.; Robb, M. A.; Cheeseman, J. R.; Montgomery, J. A.; Vreven, T.; Kudin, K. N.; Burant, J. C., Gaussian 03, Revision B. 03. Gaussian, Inc., Pittsburgh, PA. Google Sch. **2003**.
- [31] Toxvaerd, S.; Heilmann, O. J.; Dyre, J. C., Energy conservation in molecular dynamics simulations of classical systems. *J. Chem. Phys.* **2012**, *136*, 224106-8, DOI: 10.1063/1.4726728.
- [32] Morsali, A.; Goharshadi, E. K.; Ali Mansoori, G.; Abbaspour, M., An accurate expression for radial distribution function of the Lennard-Jones fluid, *Chem. Phys.* **2005**, *310*, 11-15. <https://doi.org/10.1016/j.chemphys.2004.09.027>.
- [33] Goharshadi, E. K.; Akhlamadi, G.; Mahdizadeh, S. J., Investigation of graphene oxide nanosheets dispersion in water based on solubility parameters: A molecular dynamics simulation study. *RSC Adv.* **2015**, *5*, 106421-106430. <https://doi.org/10.1039/c5ra19932h>. 10.1039/C5RA19932H.
- [34] Ghatee, M. H.; Zolghadr, A. R.; Moosavi, F.; Pakdel, L., The extent of molecular orientation at liquid/vapor interface of pyridine and its alkyl derivatives by molecular dynamics simulation. *J. Chem. Phys.* **2011**, *134*, 74707. <https://doi.org/10.1063/1.3554361>.
- [35] Ghatee, M. H.; Moosavi, F.; Zolghadr, A. R., molecular dynamics simulation studies of some new aspects of structural and dynamical properties of N-butyl formate at varying temperature. *J. Mol. Liq.* **2012**, *167*, 5-13. <https://doi.org/10.1016/j.molliq.2011.11.016>.
- [36] Zakharchenko, K. V.; Katsnelson, M. I.; Fasolino, A., Finite temperature lattice properties of graphene beyond the quasiharmonic approximation. *Phys. Rev. Lett.* **2009**, *102*, 046808, DOI: 10.1103/PhysRevLett.102.046808.
- [37] Neek-Amal, M.; Peeters, F. M., Lattice thermal properties of graphane: Thermal contraction, roughness, and heat capacity. *Phys. Rev. B* **2011**, *83*, 235437, DOI: 10.1103/PhysRevB.83.235437.